

Global property prediction: A benchmark study on open source, perovskite-like datasets

Felix Mayr¹ and Alessio Gagliardi ^{*1}

¹Department of Electrical and Computer Engineering, Technische
Universität München, München, Germany

October 21, 2020

Abstract

Screening combinatorial space for novel materials - such as perovskite-like ones for photovoltaics - has resulted in a high amount of simulated high-throughput data and analysis thereof. This study proposes a comprehensive comparison of structural-fingerprint based machine-learning models on seven open-source databases of perovskite-like materials to predict bandgaps and energies. It shows that none of the given methods are able to capture arbitrary databases evenly, while underlining that commonly used metrics are highly database dependent in typical workflows. In addition the applicability of variance selection and autoencoders to significantly reduce fingerprint size indicates that models built with common fingerprints only rely on a submanifold of the available fingerprint space.

Introduction

Perovskite-like materials are of paramount interest in the creation of novel photovoltaic devices. While existing perovskite materials, such as $\text{CH}_3\text{NH}_3\text{PbI}_3$ are unstable and/or contain toxic lead [1, 2], the available, combinatorial space of possible candidate compounds is extensive [3]. This is especially interesting when considering mixtures and different structural phases, which might have widely varying properties [4, 5]. Notably for binary mixtures of selected ions, it is already well established that the relation between an experimentally measured property (e.g. the bandgap) and material concentrations can be fit with simple, analytic functions [5, 6]. With the industry-led rise of machine-learning-(ML)-methods, there has been growing interest to predict such relationship in the high-dimensional space of all possible compounds using ML techniques [7, 8].

While these approaches have been used for years in engineering and science in general [9], the widespread application in computational materials science is relatively new and accompanied by the (re-)development of a wide range

*alessio.gagliardi@tum.de

of “fingerprinting functions” [10–20]. These are necessary to encode the typical atomic and structural information describing materials of interest into a numerical vector format necessary for common ML-techniques. For modeling computationally heavy quantum-chemistry calculations, two major approaches can be discriminated. In the first, one tries to replace certain parts of already established frameworks with ML-models, e.g. the parametrization of molecular forcefields [21, 22] or the density functional in DFT [23]. The second approach tries to create a surrogate model for prediction of materials properties given only the fingerprints as an input; typical properties for prediction with such a surrogate model are: stability/formation energy-terms [12, 19, 24–27], bandgaps [7, 19, 28–33] or even specific medication properties [34]. Recent efforts also focus on the prospects of creating “new” materials from generative models or directly feeding the structural graph to a neural-network approximator [35–37].

This study focuses on the surrogate model approach applied to crystalline, perovskite-like materials. In this field, most new methods or supposed performance improvements are only demonstrated with proprietary or novel datasets, severely limiting comparability to preexisting approaches and effectively hindering objective assessment of method performance across the field [28, 32, 38]. This is a direct result of the lack - to the author’s knowledge - of a generally accepted, consistently annotated and high-quality benchmark database for crystalline materials, which could be used for benchmarking of new methods, like GDB-17 and its offspring QM9 are for organic systems [39, 40]¹. It should also be noted here that diverse databases - inevitably necessary for a complete surrogate model - tend to generate very large fingerprint vectors, which pose a theoretical and practical problem, when the size of the fingerprint is larger than the number of datapoints available for model building, possibly deteriorating performance [43].

Most studies seem to implicitly employ both the regularizing properties of ridge-regression, as well as the (arbitrary) “metric” induced by a kernel function and do not warrant further attention to this problem [17, 19, 32].

Herein, a typical materials science surrogate modeling approach (compare Figure 1) employing Kernel-Ridge-Regression (KRR) is used on a variety of pre-existing high-throughput databases of various crystalline, perovskite-like materials [19, 32, 44–47]. A host of different fingerprinting functions are compared [13, 16, 17], including an improved, competitive version of the Property-Density-Distribution Function (PDDF)[19].

To assess the influence of KRR in squashing the dimensionality of the problem, this study employs a statistical feature selection process using variance thresholding and dimensionality reduction with neural-network autoencoders [19, 48].

The results underline that actual model accuracy as commonly published depends strongly on the dataset. Intra-dataset even varying methodologies does yield comparable results within the estimated errors for bandgap predictions, while no single method is able to create equally accurate models for all datasets. Analysis of the fingerprints reveals that models only rely on a subset of the available information in each at the given dataset scales.

¹This might also be correlated to the prevalence of Kernel-Ridge-Regression (KRR) based methods [24, 41, 42], which scale badly with very large (>100k samples) databases, such as from the OQMD-project.

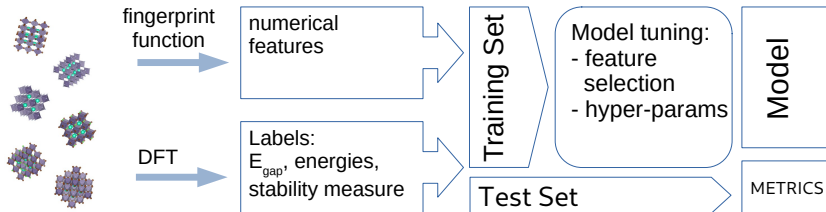


Figure 1: A typical materials prediction workflow for building a surrogate using structural fingerprints. The cost of DFT is typically magnitudes higher than for model evaluation or fingerprinting.

Methods

A typical property-predicting ML surrogate model for materials science is created in a supervised-learning setting on a sufficiently large set of (atomic structure, property)-tuples. The arguably most simple way to do this, is to take basic compositional information, such as the fractional part of constituents, and then either fit a classic (non)-parametric model or train an artificial neural network (ANN). A natural next step is to use means and higher moments of the property distribution over all atoms in a given structure as a numerical input vector, which yields surprisingly good results although it is completely insensitive to any structural differences [49]. For a constrained space of the input structures, which follow a given chemical structure (such as the perovskite-like ABX_3 -one), one can also do this in a fine-grained “per-site” way and include basic structural information [31, 33].

Although this has also been used for structurally diverse perovskites, this study will focus on fingerprints, which allow incorporation of structural information independent of a predetermined system. Notably this includes the sine-matrix [16], the Smooth Overlap of Atomic Positions fingerprint (SOAP) [13, 41], the many-body-tensor-representation (MBTR) [17] and the property density distribution function (PDDF) [19], leaving out approaches only commonly employed with molecules and various adaptations of local atomic symmetry functions [10–12, 15, 18].

Except for the Coulomb-matrix-derived sine matrix [12], all employed descriptors are derived from a shared basis, where for a given atom j , the environment is described by the atomic density of its neighbors i (see [13, 41])²:

$$\rho_j(\vec{r}) = \sum_i \delta(|\vec{r} - \vec{r}_i|). \quad (1)$$

Also, as this formalism is “atom-centered”, any derived, numerical fingerprint is atom-local first and it is necessary to transform it to a “global” fingerprint to be used for predicting system-total properties for systems of varying compositions. This transformation is done using special kernel-functions with kernel-based ML-techniques [41] or by averaging the output over all atoms [19, 42, 50].

²NOTE: even for this very simple fingerprint formalism, one could replace the δ -function with a more continuous, Gaussian-like one, add specific weights for specific neighbor atoms i and add a cutoff-function f_c , which limits the range, where $\rho > 0$.

While the SOAP fingerprint consists of the coefficients for expansion of the atomic density with radial and spherical basis functions, both MBTR and PDDF extend upon classic radial distribution functions. Within the MBTR approach, both partial radial and angular distribution functions can be parametrized on different scales. On the contrary, the PDDF weights contributions to a global RDF with atomic properties. A thorough review of all used methods can be found in the SI.

A common problem with SOAP and partial RDF-based fingerprints is that they tend to generate large ($\mathcal{O}(1000)$) fingerprint vectors, which – when combined with a non-regularizing regression method – could lead to model overfitting if the dataset is also in the lower $\mathcal{O}(1000)$ -range and require large amounts of computational resources for kernel computation. While sparsity of the individual fingerprints and the regularization part of KRR seem to alleviate this concern in a non-explicit way in most previous studies, this study employs variance-selection to methodologically shrink the input feature vector and observe the influence on surrogate modeling.

Additionally, dimensionality reduction techniques are employed to shrink the fingerprint vector, reducing the risk of overfitting and computational cost as well. The underlying assumption is that for most small-scale datasets, the structural and compositional variation within certain restrictions (such as: “only perovskite-like” materials) is changing fingerprints in such a way, that this change can be projected onto a lower-dimensional manifold.

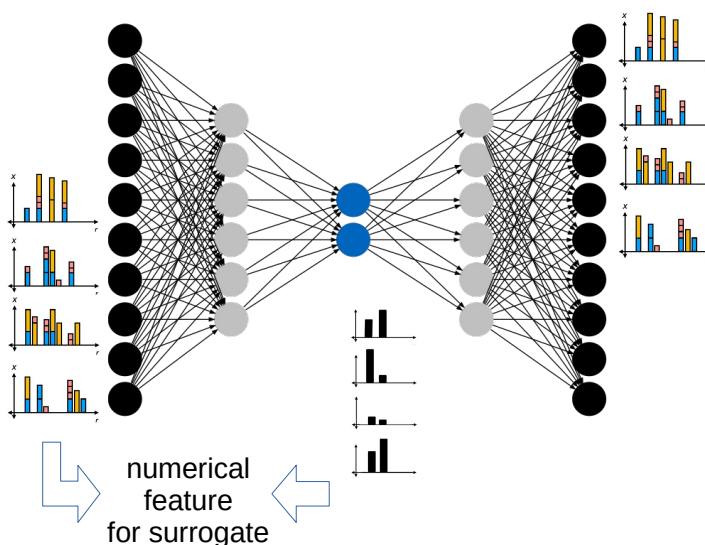


Figure 2: Network architecture of a 2 layer-autoencoder. The input is a numerical vector, the output tries to reconstruct the input, passing through a bottleneck, the so called “latent space” (blue). Surrogate models are then either built on top of the input or the intermediate representation.

For this purpose this work proposes to use autoencoders, which are an unsupervised learning method using neural networks, passing the fingerprint as an input through an “encoder” network leading up to a “latent”-layer (which

is smaller than the original) and then up again through a mirrored network (the “decoder”) such that the original input is recreated (see Figure 2). For building a regression model, the encoder then creates a compressed representation of all the fingerprints in question and these are fed to classical Kernel-Ridge-Regression. Furthermore, one could - depending on the design of the study - feed all candidate compounds to the autoencoder including the ones, where one would like to do ML-based predictions (because training it is much cheaper than running full DFT for all). Also, the reduced and ideally non-sparse feature-vector could allow to optimize for fingerprints (and subsequent structures) with a desired property within the restricted compositional and structural space of an numerical experiment [36].

Data

The availability of consistent, high-quality data is crucial for building a ML model and eventual benchmarking of different modeling approaches. Due to the lack of a shared, reproducible benchmark with a lot of common materials properties in the “solid-state”-community, authors tend to create their own datasets, when publishing new methods or researching new problems [28, 32, 38]. This process introduces the danger of the data being biased in an inadvertent way and thus giving unrealistic, non-generalizable results. In addition, creating a suitable, high-quality DFT database of crystalline solids is a challenging task itself: one would like to have a high-fraction of “physical” systems, e.g. at their minimal energy, which requires extensive structural relaxations or even metadynamics to sample different likely substructures [47]. Calculations should also use a shared set of sufficiently exact parameters for all calculations to converge, which is hard to achieve with varying cell-sizes and some of the proposed inputs exhibiting metallic behavior. Once a suitable amount of structures is relaxed, it still has to be assured that the model relates to physical reality, e.g. in the case of the bandgap as a property by incorporating spin-orbit-coupling and hybrid DFT, which generally seems to give bandgaps in good agreement with experiments compared to the underestimation by GGA [51, 52].

While creating a high-quality database taking into account all these considerations is necessary to create a useful, physically exact surrogate model, for methodological development the usage of datasets of lower complexity is definitely possible. Although a PBE-trained model might not yield accurate property values it can be expected that model accuracy will not get worse than the PBE baseline - which is still used for screening today - when trained on hybrid training data, while possibly leading to a significant performance increase. Thus herein the choice fell on existing datasets of varying provenance and methodological backgrounds to assess whether the given methods are able to build effective surrogate models across different databases - a mutual theme is the inclusion of perovskite-like structures [19, 32, 44-47].

A large ($\approx 19k$ samples) dataset of cubic perovskites is used from [44, 53]. It consists of cubic oxide-perovskite-scaffolds, featuring a wide range of cations and fractional replacement of the oxygen with fluorine, nitrogen and sulfur. Optimized cubic-structures were found by scanning a range of lattice parameters and relaxing the resulting structure using DFT with the RPBE-functional. For all non-metals, direct and indirect bandgaps were subsequently calculated with

the GLLB-SC functional, which yields good agreement with experiments. A subselection of these compounds (only with O and N-anion) and the same methodology were employed to derive a database of Ruddlesden-Popper layered-perovskites [45].

Compared to these basic databases mainly varying the composition, the “hybrid organic-inorganic perovskite-dataset” by [47] includes molecular cations A in a “classic” ABX_3 -halide-perovskite-scaffolds (with $B=Ge/Sn/Pb$ and a halide X). Basic scaffold structures and cells were selected by running a minima-hopping simulation for initial $ASnI_3$ -compounds resulting in a large number of different structural motifs, replacing the other sites and running a structural relaxation with the rPW86-functional. Bandgaps were then evaluated with the final structures at the position of both the direct and indirect gap in the relaxation calculation using hybrid DFT (HSE06).

In addition, a database of A_2BCX_4 -type materials was selected [46], which are similar in size and scope to typical double-perovskites. Structures are based on six different prototypes with the composition determined by empirical rules. Structures were optimized using PBEsol, with meta-GGA then used for energy calculations and GLLB-SC for accurate bandgaps.

Two smaller databases based on plain GGA and simple relaxation of base structures are also included: first, a recently published dataset based on experimentally available 2D-perovskite compounds [32]. The structures therein generally resemble surfaces and thus exhibit widely varying cell-sizes³. Second the database used by the authors in the introduction of the PDDF, consisting of relaxed, lead-free, inorganic mixed $2 \times 1 \times 2$ -cubic-cell perovskites calculated at the GGA-level using an LCAO approach even for bandgaps is included [19].

As all these databases incorporate a wide variety of species, fingerprints treating each pair of possible species separately (SOAP, MBTR) might be at a disadvantage and thus the crystalline dataset used in the Nomad-2018-Kaggle-competition consisting of a wide variety of $(Al_xGa_yIn_{1-x-y})_2O_3$ -compounds was included as a further reference [42].

A basic overview of core properties of all used databases is found in Table 1, including summary statistics over all datapoints for structure size and the type of the bandgap/energy property. Note that these properties are not comparable inbetween different databases.

ML Experiments

In order to facilitate the comparison objective, the property prediction workflow is standardized across all databases and no dataset-tailored parameters or methods beyond the statistical model fitting/training procedure are used (see Figure 1). First, each randomly shuffled dataset is split into a 80%-set for training and validation, while the remaining 20% is set aside for testing. Then the chosen fingerprinting function is applied to the structures, feeding the output either to an intermediate step reducing the fingerprint with an autoencoder or variance selection, or directly building the model using the fingerprints and a selected global property as a target. For all models, 5-fold cross-validation was used to tune hyperparameters of a Kernel-Ridge-regression model using radial basis

³the reader should be aware that this database is apparently being updated. Thus, the shown statistics only show a snapshot prior to publication of this paper (2020-07-28)

	Total compounds	unique species	size	max cell vector [Å]	avg. cell vector [Å]	bandgap [eV]
Kim [47]	1346	11	15.1 [9-21]	7.4 [4.4-11.7]	6.0 [4.3-7.6]	3.8 [1.52-6.63] (HSE06)
Pandey [46]	1341	25	19.8 [16-32]	11.9 [7.0-21.5]	7.7 [6.4-10.5]	2.1 [0.01-4.28] (GLLB-SC)
Stanley [19]	344	9	20 [20-20]	11.6 [10.9-13.9]	9.2 [8.7-9.9]	1.4 [0.35-3.08] (LCAO, PBE)
Castelli [45]	1984	47	20.9 [14-44]	10.6 [7.3-24.0]	6.6 [5.5-9.4]	3.5 [0-8.44] (GLLB-SC)
Castelli [44]	18928 [735 nonzero gaps]	56	5 [5-5]	4.1 [3.3-5.7]	4.1 [3.3-5.7]	0.1 [0-7.90] (GLLB-SC)
Marchenko [32]	445	16	48.8 [4-452]	27.7 [9.4-102.0]	13.2 [6.4-22.9]	2.4 [1.65-3.53] (LCAO, n/a)
Sutton [42]	3000	4 [4-4]	61.7 [10-80]	15.1 [9.0-28.0]	9.0 [4.8-10.8]	2.1 [0.0-5.84] (PBE)

Table 1: Overview of the used databases. Size (number of atoms), length of the maximal/geometrical average cell-vector (Å) and bandgap are all given in the format: “mean [minimum - maximum]”. In parenthesis, for the bandgap, the chosen exchange functional is given.

functions. Finally, the resulting model is evaluated on the test set, resulting in an estimation of prediction accuracy in Table 2 for direct bandgaps and for per-atom (formation) energies for each compound (in the SI). Each model is evaluated using the mean-absolute-error (MAE) metric to estimate the error of the prediction and the R^2 -score (coefficient of determination) to classify the adherence to the ideal (prediction = ground truth)-relation, as the MAE alone depends strongly on the dataset. The MAE-metric was deliberately chosen over the root mean-squared-error (RMSE) used in similar works [28, 54], because it deemphasizes outliers in predictions and is independent of the sample size [55]. Also for a materials prediction workflow, where the end result will be validated with high-level calculations or experiments from a relatively large array of surrogate-qualified candidates, singular predictions which are off by a large amount are less relevant. The results shown in Table 2 are the average of 10 different train-test splits with the standard deviation used as an error estimate. In face of the small datasets and non-standardized train-test-splits this method was chosen to avoid sampling a pathological, non-generalizable split [19, 54].

While nothing precludes the use of neural networks or other regression methods, Kernel-Ridge-regression was used throughout all experiments due to its low number of tunable parameters and its popularity within previous work [17–19, 32, 42, 54]. The “meta”-kernel approach was evaluated as well, specifically for the SOAP descriptor, but ultimately discarded, as it requires an enormous amount of computational time for kernel evaluation, while only marginally improving results [41, 50].

Although there is a magnitude of “global”, macroscopic properties available [24], the employed databases only include bandgap and energy measures. While the bandgap can be used “as-is” as a global property and is comparable except for intrinsic differences in the methods accuracy between databases, energy measures vary, with the availability ranging from bare total DFT-energies to formation energies within different, non-comparable frameworks. Remedying this would require recalculating all compounds in a shared framework, which is beyond the scope of this study. Thus, the focus lies upon the bandgap prediction models, with performance of prediction models for different kinds of formation energies and intensive “per-atom”-DFT-energies shown in the SI.

To assess a baseline performance level for the more advanced methods this study includes the results of a dummy-regressor, returning the mean of the training dataset for all “predictions” on the test set. Only on the hybrid perovskite database [47], some handpicked features (8 features: avg., site-specific properties for the ions [28, 49]) were considered and show a relatively good model ($R^2 \approx 0.79$) with a MAE of ≈ 380 meV for the bandgap. At this point it becomes apparent that the MAE alone gives no real indication for the quality of a surrogate model. For example the dummy-regressor on the Marchenko database [32] achieves a similar “performance” as the primitive predictor on the Kim-database [47], which already improves significantly on the dummy-prediction there, both with the MAE and the R^2 -score. With the bandgap prediction, creation of a decent ($R^2 \simeq 1$) model for the full dataset of cubic perovskites [44] was not possible and thus the subset of perovskites with non-zero bandgaps was selected for modeling [28].

For the SOAP-fingerprint, the sparse, single-constituent fingerprints of a crystal were taken and averaged to create a global descriptor [42, 50]. The

parameters used in fingerprint creation⁴ were picked from the existing literature, where widely varying numbers for the modeled cutoff radius and the number of radial and spherical basis functions are given without any reasoning (see the SI for a listing) [13, 32, 41, 42]. Assuming that large systems (such as in [32, 45]) might benefit from modeling a larger cutoff radius around individual atoms, the parameters from [32] were also included with a radius of 16Å.⁵

Kernel-calculation for the full fingerprints is very compute-intensive with fingerprint size in the 5-digit range depending on the number of species included in the data. Thus individual features were min-max-scaled to the [0, 1]-interval and variance selection with a 0.01 threshold was employed to significantly reduce the fingerprint size before scaling the data to unit-variance and feeding the data to a KRR model using radial basis functions. Resulting models match or exceed performance of the usage of the full-fingerprint, where a simple linear kernel and no scaling were used as the radial basis function kernel required more computational time and didn’t improve accuracy.

For the MBTR, only the k_2 -part was used, as this already results in a sizable fingerprint of size $s^2 \cdot b$, where s is the number of species in the database, while b is the number of discrete bins, used to discretize the fingerprint on the given cutoff-radius of 16 Å⁶. $b = 10$ was chosen and worked well with both the partial-rdf-equivalent representation as well as discretization over the inverse-radius and no scaling applied before feeding the data to the radial-basis KRR-model. Using both, the full MBTR including the angular parts, as well as setting $b = 100$ for the k_2 -version [17, 54] did not produce improved results consistently and significantly increased computational time. Applying the same variance selection process used with SOAP did not provide improved results either.

Finally for the PDDF, different discretizations were explored for a radius of 16 Å and a total of 8 properties. With an amount of 160 features discretized with 0.8 Å-bins and a gaussian spreading of 1 Å, the PDDF already works in building a bandgap model for all datasets – except the cubic perovskites – when scaled to standard variance. A finer discretization with 0.1 Å-bins for the PDDF results in markedly improved results, while increasing the number of features 8-fold (1280). Using a simple, 1-layer linear-activation autoencoder architecture trained on the [0, 1]-scaled PDDF-representation of the training data alone, allows encoding the fingerprint into a 160-feature representation again. Using this representation with KRR consistently reaches the performance of the full representation hinting that the PDDF-fingerprint indeed represents a low-dimensional manifold describing the data. Further studies could be conducted to explore whether and how the latent space is actually a representation of this manifold and how it relates to basic input structural data. In a similar vein, Schrier [56] explored the eigenspectrum of the Coulomb-Matrix fingerprint for molecular data and found, that even this already shrunken representation can be further reduced.

Detailed results can be found in Table 2 for the bandgap and the SI for

⁴these could be thought and optimized as hyperparameters of the whole “machine” – though this hinders general applicability and requires expensive remodeling for new data

⁵Note that the dataset in [32] is proprietary and based on a subset of the available database, so the results are not directly comparable.

⁶This specific radius was chosen so it captures the environment of the maximum “whole cell” for most compounds (compare with the cell-vector geometrical average and maximum unit-cell vector lengths in 1). Also it could be discretized conveniently for numerical experiments as a multiple of 2.

energy predictions and the remaining SOAP and MBTR-related experiments.

Evaluation

For all of [19, 42, 46, 47], both the PDDF-approach and SOAP yield comparable prediction accuracy below 120 meV MAE with a slight lead for the SOAP fingerprint. In case of the PDDF, both increasing the number of discretization steps and using the weighting proposed by [57] considerably improve results compared to the original rediscovered approach [19]. Against that, the results of the SOAP method seem relatively independent of parametrization in spherical and radial basis functions. Prediction is neither changed by decreasing the smearing of the atomic positions (“+fine”-attribute), but for [19, 46] increasing the radius expanded in the fingerprint results in a marked improval. The sine-matrix approach is only significantly improving on the dummy-predictions in the case of constant system size [42] or with the hybrid perovskite dataset incorporating a high number of atoms for all systems [47]. Except for [42], all MBTR-parametrizations lag behind, regardless of the specific setup. While all best-performing prediction MAEs are of similar magnitude, it is notable that the baseline differs: for [42, 46, 47] the error of educated guessing is ≈ 800 meV, whilst it is only ≈ 300 meV for [19].

Conversely, for [45] the MBTR-representation discretized on the inverse-radius-grid shows the best results, albeit model quality measured with the R^2 -coefficient doesn’t reach the best results of the previously discussed datasets and the best MAE is nearly doubled to 250 meV. Both SOAP and the PDDF are performing worse for this datasets.

Similar, for the large-cell data from [32], the PDDF approach performs worst, independent of parametrization. With errors of 130 meV and 140 meV respectively, SOAP and MBTR are leading, though compared to the other databases with comparable MAEs, this is a considerably smaller improvement on random guessing!

Finally for the cubic perovskites [44], no model reaches a satisfactory R^2 even with the dataset reduced to non-metallic compounds only. MBTR leads the field with an MAE of 700 meV followed by SOAP and the PDDF in 50 meV increments. Here, the proposed methods for building a surrogate model seem to fail, possibly a result of the discontinuous nature of the input structures just being the results of simple combinatorics. Thus, for the sparse SOAP and MBTR-fingerprints, most features just are incomparable with some parts being non-zero only in singular samples.

Overall, as visualized in Figure 3 and further shown for all parametrizations in the SI, the exact choice of specific fingerprinting parameters or even the basic method has a much less produced effect on resulting errors than the choice of the database. Even for technically very pathological parametrizations, e.g.: smoothing distributions with Gaussians of a similar width as the distribution range or the opposite for SOAP, the errors do not change on the order of magnitude. While this study did not perform any large scale fingerprint hyperparameter tuning [54] – instead choosing to replicate previous studies methodology, spanning a wide range of parameters – this indicates that for most practical screening applications the choice of method is less important than having a “suitable” database. “Suitable” in this case goes far beyond the addition of

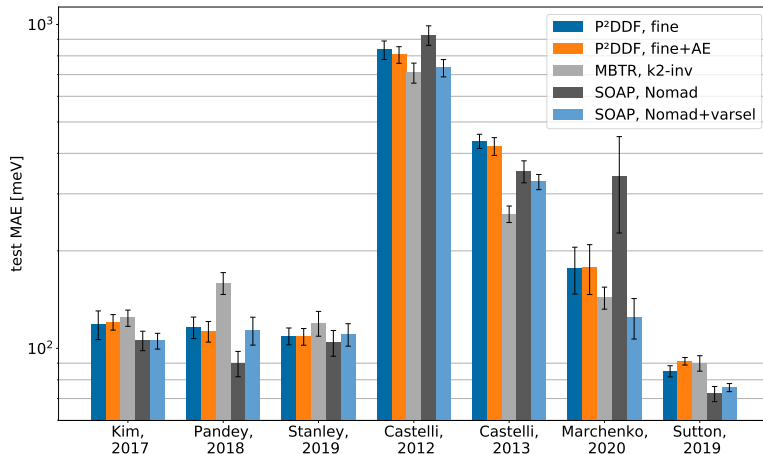


Figure 3: Bandgap prediction error visualized for selected model across all databases

new datapoints, as the failure of building a very good model for the data from [44] and [45] shows. While one might attribute this to the high amount of unique species in these datasets (see Table 1), comparison between the similar results for the data from [47], [46], [19] and [42] shows that this is not the only deciding factor. This becomes especially apparent in the direct comparison of [47] and [46], where the number of available compounds is similar, yet the number of unique species is much higher in [46].

To provide further insight into model quality and limitations, Figure 4 and 5 provide learning curves and error-distributions for the bandgap prediction on the data from [46]. The curves plot the average MAE of models evaluated on a 20% test set versus the fraction of the respective training set used for creating the model. All fingerprint methods and feature extraction techniques show a consistent improvement with increasing training data with no sign of flattening out, indicating that more training data could be used to further improve model quality. In the low-data-regime, MAEs are exceeding 250 meV and the models based on the autoencoded PDDF as well as the variance selected SOAP significantly trail the pure, small-bin PDDF. By increasing the amount of data used for model creation, both SOAP and Autoencoder-model performance reach parity with usage of the full PDDF in model creation. The autoencoder results could be related to a biased sampling which is not able to fully capture all structural features available in the dataset. In a real prediction setting, one might thus include a larger array of prospective compounds, including the finally predicted datapoints for training the autoencoder.

Checking the error distributions for different best-case results with a 80/20-train/test-split shows gaussian like distributions, so there is no inherent bias of any of the tested modeling procedures (compare Figure 5).

Additionally, in a first effort to understand the effects of the autoencoder on the PDDF-fingerprint vectors used as input in the KRR model, t-SNE embed-

	Kim [47]	Pandey [46]	Stan. [19]	Cas. [44]	Cas. [45]	Mar. [32]	Sutton [42]
handpicked	381±11	-	-	-	-	-	-
dummy	884±34	730±19	323±23	1270±73	1530±46	332±15	845±16
sinematrix, eigenspectrum	368±15	538±39	212±15	1088±77	1102±60	298±22	141±8
PDDF, basic	172±11	199±13	134±11	930±80	551±16	179±11	101±4
PDDF, fine	141±8	139±14	114±12	888±57	481±19	176±20	90±4
PDDF, fine+AE	142±6	143±7	110±12	879±61	490±28	170±19	91±4
P ² DDF, basic	159±12	172±14	136±19	888±69	521±19	207±32	96±3
P ² DDF, fine	118±12	116±9	109±7	834±55	436±22	176±29	85±3
P ² DDF, fine+AE	120±7	113±8	109±6	806±48	421±27	178±31	91±2
MBTR, k2-inv	124±7	159±12	120±11	709±50	260±15	143±11	90±5
MBTR, k2-rdf	128±7	144±13	126±10	786±57	305±18	140±18	93±6
SOAP, Marchenko	100±8	85±9	109±7	1067±75	349±27	494±90	70±5
SOAP, De	107±6	97±9	108±8	1071±74	329±25	442±95	78±4
SOAP, Nomad	106±7	90±8	104±10	926±64	352±27	339±112	72±4
SOAP, Marchenko, LR	110±11	96±7	122±10	1288±130	645±58	939±330	75±3
SOAP, Marchenko+varsel	101±6	111±10	123±8	738±52	309±24	132±17	77±6
SOAP, De+varsel	106±9	112±10	116±7	777±50	339±23	135±20	78±4
SOAP, Nomad+varsel	105±6	114±11	110±9	734±45	327±18	125±18	76±2
SOAP, Marchenko, LR+varsel	99±8	90±5	104±8	745±48	324±27	129±25	76±3

Table 2: Results for predicting the calculated bandgaps for different methods, all results in meV for the mean-absolute error (MAE). The parameters for specific identifiers are listed in the supporting information. Note here, that P²DDF is used as a shorthand for the product-weighting proposed by [57]. `varsel` indicates that the machine learning was trained on the variance selected features of the specified fingerprint function

dings are used to create a 2-dimensional map of the relative “neighborhoods” accessible in the fingerprint (see Figure 6) [58, 59]. The dataset from [47] was used because it has a clear ABX₃-perovskite structure and a relatively well working model, so a relation to physical quantities is relatively easy. When overlaying the bandgap on a plot of the first two t-SNE dimensions, it is evident that the autoencoder preserves information about the physical characteristics of the system and the resulting models are no statistical artifact compared to using the PDDF. In the example, it even seems like the autoencoded representation is able to capture the bandgap-landscape in a much more continuous way than the original fingerprint, where a large number of singular high bandgap values are interspersed in the t-SNE-map. This observation can be related to the fact that the autoencoded representation clusters depending on A and X-sites (see SI for the t-SNE-plots for A, B and X-site-“occupation”), with the B site not clearly distinguishable as separate clusters in 2D. Conversely, the raw fingerprint does cluster mainly by the B and X-occupation, while the molecular ions at the A site are not distinguishable in 2D clusters. As previous studies have shown that the B-ion is not very relevant for the bandgap [19, 60], this hints that the autoencoder might actually be able to extract a “chemically informed” representation from the fingerprints. Obviously, the realizable advantage of this in building ML surrogates may be limited, as these are generally built on a space with a much higher dimension and the model can exploit more complicated relations than visualizable in a 2D map.

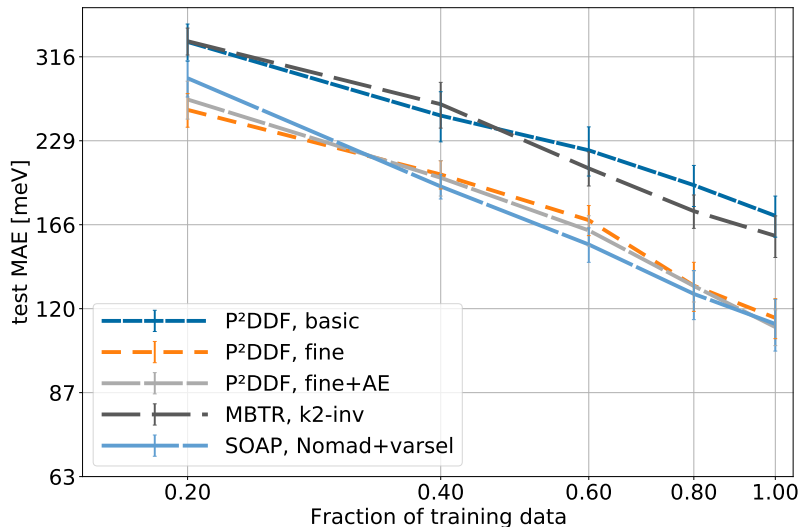


Figure 4: Learning curves for the data from [46]. Shown is the test MAE for selected machine learning models.

Conclusion

The key takeaway of this study is that all currently competitive methods to create surrogate models for the prediction of materials properties are not able to capture arbitrary databases evenly yet. While a fraction of this might be attributed to varying complexity of the databases, the utter failure to capture a “good” bandgap-model in the conceptually very simple, large database of cubic perovskites [44] hints that these methods in their commonly used form are not fit to replace DFT to model “discontinuous” relationships, where one just replaces a single atom with another compound-unique-species (a finding evident already in the authors previous work [19]). However, for varying “alloys” and superstructures in a more or less continuous way, such as it happens in the other databases, as well as in [42], the outlined methods seem to be able to perform quite well; a MAE of around 100 meV is great, comparing the inherent inaccuracies of experiments and DFT (GGA vs. hybrids) [61].

Additionally, for all studied descriptors, this study could not establish a strong, order-of-magnitude variation in per-dataset model performance for varying parameters within the boundaries of previously published work, hinting that for all practical applications, a finegrained hyperparameter search [54] might be inefficient. Across all datasets, no method consistently reached best performance, though SOAP is leading for several datasets. Setting aside different modeling techniques for the raw data, the available results for the bandgap models also indicate that choosing a method, much less choosing appropriate parameters for it, has much less influence than choosing a dataset. Thus these findings question the significance of performing studies on isolated, proprietary datasets aiming for ever better numerical results without establishing baseline

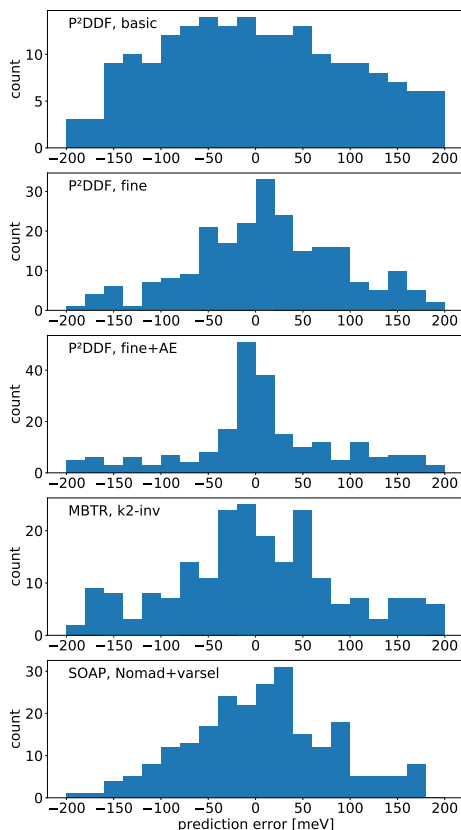


Figure 5: Error distribution for the best performing models for the data from [46] for selected machine learning models

performance metrics and a comparison framework [31–33].

From a technical perspective, the fact that fingerprinting functions creating input vectors of a length several times the samplesize work so well is a bit puzzling. Normally one would expect a strong overfitting to the test set, as the models have more free parameters than fitted samples. While that is exactly the reason for using a regularizing ML method, such as Kernel-Ridge-Regression (KRR), the high sparsity of both the SOAP and MBTR-fingerprint for highly diverse databases could as well mean that the model that way only learns from a fraction of the supplied input data as shown in [62]. The results of this study, which show SOAP with simple variance-based filtering of input features leading the field, underline this problem. This should warrant further investigation, as it also means that the given model will never be able to achieve full DFT accuracy just learning the substructure of e.g. O, F and N-atoms, which incidentally are the shared building blocks of the cubic perovskite set, where MBTR excels but has a accuracy which is in a range comparable with compounds swapping the A and B ions [60].

It should also be noted that original authors open-sourcing their data or even publishing ML-models should include a recommended training/test-split

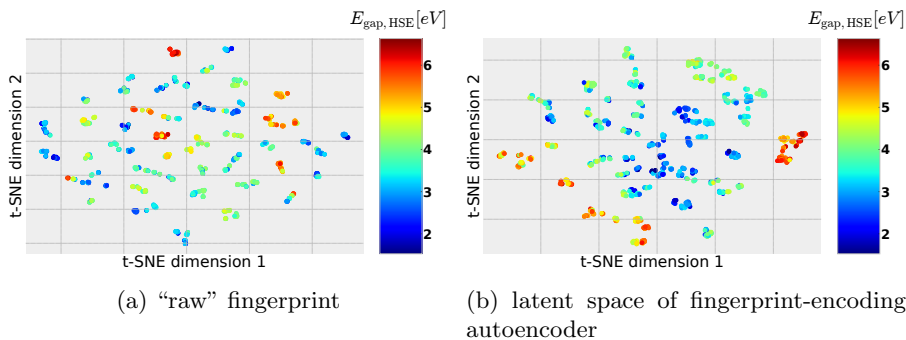


Figure 6: t-SNE reduced PDDF fingerprint and its encoding in 2D. Bandgap overlaid and colorcoded to relate to physical realities.

so that results between methods can be compared across different publications [20]. This is especially important, as the usage of neural networks in innovative ways slowly reaches the materials science field. With graph neural networks (GNN) already beating the established fingerprinting procedures easily on the GDB-17-derived databases [63, 64] so the field can expect further inquiries, for which good and standardized data is a necessary requirement. The applicability to the solid-state field currently is mostly hampered by small databases of relevant properties as the current, OQMD-derived databases only include formation energies in a consistent, high-quality format and are mostly metallic [37, 65]. Such developments might also be necessary to escape the fact that actual model performance is more tied to the data than to the model, which looks eerily similar to the state of natural-language-processing 20 years ago [66].

The availability of such large-scale databases could also facilitate a more detailed examination of dimensionality reduction and its workings. While this study shows that the PDDF-fingerprint seems to incorporate information on a low-dimensional manifold for the given datasets and this information in fact allows to construct models of equivalent quality, it is not clear, whether this approach can be further improved and yield extended insights. t-SNE-analysis hints that the encoding preserves “chemical information” while significantly reducing the feature size. Thus it eases the systematical optimization of the resulting surrogate model in search of new compounds but it is unclear, whether it is thus possible for the model to actually relate to properties of physically realizable compounds.

Tools

All calculations were done in a PYTHON-environment using the NUMPY, PANDAS and ASE packages for basic data manipulation and structure file handling; plotting was done with MATPLOTLIB. Machine learning procedures were used/implemented with SKLEARN and TENSORFLOW, while the fingerprints were generated with DESCRIBE[50] and our own implementation of the PDDF. Code to reproduce all numerical experiments is available upon request from the authors.

Supporting Information

The supporting information includes a tabular overview of all fingerprint parameters for numerical experiments. Also, MAEs, R^2 -scores and RMSEs are included for the subpar-performing fingerprints on the bandgap prediction and for all energy prediction models.

Additional experiments on the data from [46] are included to show that for the PDDF, published performance of the fine-grained approach can not be reached with single-property PDDFs alone.

Acknowledgments

The authors thank Waldemar Kaiser for a diligent reading of the late draft.

References

- ¹G. Niu, X. Guo, and L. Wang, "Review of recent progress in chemical stability of perovskite solar cells", *Journal of Materials Chemistry A* **3**, 8970–8980 (2015).
- ²C. C. Boyd, R. Cheacharoen, T. Leijtens, and M. D. McGehee, "Understanding degradation mechanisms and improving stability of perovskite photovoltaics", *Chemical Reviews* **119**, 3418–3451 (2018).
- ³M. Saliba, "Polyelemental, multicomponent perovskite semiconductor libraries through combinatorial screening", *Advanced Energy Materials* **9**, 1803754 (2019).
- ⁴J.-W. Xiao, L. Liu, D. Zhang, N. D. Marco, J.-W. Lee, O. Lin, Q. Chen, and Y. Yang, "The emergence of the mixed perovskites and their applications as solar cells", *Advanced Energy Materials* **7**, 1700491 (2017).
- ⁵M. Konstantakou and T. Stergiopoulos, "A critical review on tin halide perovskite solar cells", *Journal of Materials Chemistry A* **5**, 11518–11549 (2017).
- ⁶J. J. Gallardo, M. Rodríguez-Fernández, E. Blanco, J. Outón, and J. Navas, "The effect of a complex a-site cation and mixed halides in the emission properties of perovskite quantum dots", *Journal of Molecular Liquids* **314**, 113674 (2020).
- ⁷G. Pilania, C. Wang, X. Jiang, S. Rajasekaran, and R. Ramprasad, "Accelerating materials property predictions using machine learning", *Scientific Reports* **3**, 10.1038/srep02810 (2013).
- ⁸L. Zhang, M. He, and S. Shao, "Machine learning for halide perovskite materials", *Nano Energy*, 105380 (2020).
- ⁹A. I. J. Forrester, A. Sóbester, and A. J. Keane, *Engineering design via surrogate modelling* (John Wiley & Sons, Ltd, July 2008).
- ¹⁰D. Rogers and M. Hahn, "Extended-connectivity fingerprints", *Journal of Chemical Information and Modeling* **50**, 742–754 (2010).
- ¹¹J. Behler, "Atom-centered symmetry functions for constructing high-dimensional neural network potentials", *The Journal of Chemical Physics* **134**, 074106 (2011).

- ¹²M. Rupp, A. Tkatchenko, K.-R. Müller, and O. A. von Lilienfeld, “Fast and accurate modeling of molecular atomization energies with machine learning”, *Physical Review Letters* **108**, 10.1103/physrevlett.108.058301 (2012).
- ¹³A. P. Bartók, R. Kondor, and G. Csányi, “On representing chemical environments”, *Physical Review B* **87**, 10.1103/physrevb.87.184115 (2013).
- ¹⁴K. T. Schütt, H. Glawe, F. Brockherde, A. Sanna, K. R. Müller, and E. K. U. Gross, “How to represent crystal structures for machine learning: towards fast prediction of electronic properties”, *Physical Review B* **89**, 10.1103/physrevb.89.205118 (2014).
- ¹⁵K. Hansen, F. Biegler, R. Ramakrishnan, W. Pronobis, O. A. von Lilienfeld, K.-R. Müller, and A. Tkatchenko, “Machine learning predictions of molecular properties: accurate many-body potentials and nonlocality in chemical space”, *The Journal of Physical Chemistry Letters* **6**, 2326–2331 (2015).
- ¹⁶F. Faber, A. Lindmaa, O. A. von Lilienfeld, and R. Armiento, “Crystal structure representations for machine learning models of formation energies”, *International Journal of Quantum Chemistry* **115**, 1094–1101 (2015).
- ¹⁷H. Huo and M. Rupp, “Unified representation of molecules and crystals for machine learning”, (2017).
- ¹⁸F. A. Faber, A. S. Christensen, B. Huang, and O. A. von Lilienfeld, “Alchemical and structural distribution based representation for universal quantum machine learning”, *The Journal of Chemical Physics* **148**, 241717 (2018).
- ¹⁹J. C. Stanley, F. Mayr, and A. Gagliardi, “Machine learning stability and bandgaps of lead-free perovskites for photovoltaics”, *Advanced Theory and Simulations* **3**, 1900178 (2019).
- ²⁰A. Y.-T. Wang, R. J. Murdock, S. K. Kauwe, A. O. Oliynyk, A. Gurlo, J. Brgoch, K. A. Persson, and T. D. Sparks, “Machine learning for materials scientists: an introductory guide toward best practices”, *Chemistry of Materials* **32**, 4954–4965 (2020).
- ²¹J. Behler and M. Parrinello, “Generalized neural-network representation of high-dimensional potential-energy surfaces”, *Physical Review Letters* **98**, 10.1103/physrevlett.98.146401 (2007).
- ²²J. S. Smith, O. Isayev, and A. E. Roitberg, “ANI-1: an extensible neural network potential with DFT accuracy at force field computational cost”, *Chemical Science* **8**, 3192–3203 (2017).
- ²³J. C. Snyder, M. Rupp, K. Hansen, K.-R. Müller, and K. Burke, “Finding density functionals with machine learning”, *Physical Review Letters* **108**, 10.1103/physrevlett.108.253002 (2012).
- ²⁴F. A. Faber, L. Hutchison, B. Huang, J. Gilmer, S. S. Schoenholz, G. E. Dahl, O. Vinyals, S. Kearnes, P. F. Riley, and O. A. von Lilienfeld, “Prediction errors of molecular machine learning models lower than hybrid DFT error”, *Journal of Chemical Theory and Computation* **13**, 5255–5264 (2017).
- ²⁵A. Seko, H. Hayashi, K. Nakayama, A. Takahashi, and I. Tanaka, “Representation of compounds for machine-learning prediction of physical properties”, *Physical Review B* **95**, 10.1103/physrevb.95.144110 (2017).

- ²⁶W. Ye, C. Chen, Z. Wang, I.-H. Chu, and S. P. Ong, “Deep neural networks for accurate predictions of crystal stability”, *Nature Communications* **9**, 10.1038/s41467-018-06322-x (2018).
- ²⁷M. Kaneko, M. Fujii, T. Hisatomi, K. Yamashita, and K. Domen, “Regression model for stabilization energies associated with anion ordering in perovskite-type oxynitrides”, *Journal of Energy Chemistry* **36**, 7–14 (2019).
- ²⁸G. Pilania, A. Mannodi-Kanakkithodi, B. P. Uberuaga, R. Ramprasad, J. E. Gubernatis, and T. Lookman, “Machine learning bandgaps of double perovskites”, *Scientific Reports* **6**, 10.1038/srep19375 (2016).
- ²⁹Y. Huang, C. Yu, W. Chen, Y. Liu, C. Li, C. Niu, F. Wang, and Y. Jia, “Band gap and band alignment prediction of nitride based semiconductors using machine learning”, *the Journal of Materials Chemistry C*, 2019, 10.1039/C8TC05554H (2018).
- ³⁰T. Wu and J. Wang, “Global discovery of stable and non-toxic hybrid organic-inorganic perovskites for photovoltaic systems by combining machine learning method with first principle calculations”, *Nano Energy* **66**, 104070 (2019).
- ³¹W. A. Saidi, W. Shadid, and I. E. Castelli, “Machine-learning structural and electronic properties of metal halide perovskites using a hierarchical convolutional neural network”, *npj Computational Materials* **6**, 10.1038/s41524-020-0307-8 (2020).
- ³²E. I. Marchenko, S. A. Fateev, A. A. Petrov, V. V. Korolev, A. Mitrofanov, A. V. Petrov, E. A. Goodilin, and A. B. Tarasov, “Database of 2d hybrid perovskite materials: open-access collection of crystal structures, band gaps and atomic partial charges predicted by machine learning”, *Chemistry of Materials*, 10.1021/acs.chemmater.0c02290 (2020).
- ³³H. Park, R. Mall, A. Ali, S. Sanvito, H. Bensemli, and F. El-Mellouhi, “Importance of structural deformation features in the prediction of hybrid perovskite bandgaps”, *Computational Materials Science* **184**, 109858 (2020).
- ³⁴J. M. Stokes, K. Yang, K. Swanson, W. Jin, A. Cubillos-Ruiz, N. M. Donghia, C. R. MacNair, S. French, L. A. Carfrae, Z. Bloom-Ackermann, V. M. Tran, A. Chiappino-Pepe, A. H. Badran, I. W. Andrews, E. J. Chory, G. M. Church, E. D. Brown, T. S. Jaakkola, R. Barzilay, and J. J. Collins, “A deep learning approach to antibiotic discovery”, *Cell* **180**, 688–702.e13 (2020).
- ³⁵T. Blaschke, M. Olivecrona, O. Engkvist, J. Bajorath, and H. Chen, “Application of generative autoencoder in De Novo Molecular design”, *Molecular Informatics* **37**, 1700123 (2017).
- ³⁶R. Gómez-Bombarelli, J. N. Wei, D. Duvenaud, J. M. Hernández-Lobato, B. Sánchez-Lengeling, D. Sheberla, J. Aguilera-Iparraguirre, T. D. Hirzel, R. P. Adams, and A. Aspuru-Guzik, “Automatic chemical design using a data-driven continuous representation of molecules”, *ACS Central Science* **4**, 268–276 (2018).
- ³⁷T. Xie and J. C. Grossman, “Crystal graph convolutional neural networks for an accurate and interpretable prediction of material properties”, *Physical Review Letters* **120**, 10.1103/physrevlett.120.145301 (2018).
- ³⁸J. Im, S. Lee, T.-W. Ko, H. W. Kim, Y. Hyon, and H. Chang, “Identifying pb-free perovskites for solar cells by machine learning”, *npj Computational Materials* **5**, 10.1038/s41524-019-0177-0 (2019).

- ³⁹L. Ruddigkeit, R. van Deursen, L. C. Blum, and J.-L. Reymond, "Enumeration of 166 billion organic small molecules in the chemical universe database GDB-17", *Journal of Chemical Information and Modeling* **52**, 2864–2875 (2012).
- ⁴⁰R. Ramakrishnan, P. O. Dral, M. Rupp, and O. A. von Lilienfeld, "Quantum chemistry structures and properties of 134 kilo molecules", *Scientific Data* **1**, 10.1038/sdata.2014.22 (2014).
- ⁴¹S. De, A. P. Bartók, G. Csányi, and M. Ceriotti, "Comparing molecules and solids across structural and alchemical space", *Physical Chemistry Chemical Physics* **18**, 13754–13769 (2016).
- ⁴²C. Sutton, L. M. Ghiringhelli, T. Yamamoto, Y. Lysogorskiy, L. Blumenthal, T. Hammerschmidt, J. R. Golebiowski, X. Liu, A. Ziletti, and M. Scheffler, "Crowd-sourcing materials-science challenges with the NOMAD 2018 kaggle competition", *npj Computational Materials* **5**, 10.1038/s41524-019-0239-3 (2019).
- ⁴³A. Jain and B. Chandrasekaran, "39 dimensionality and sample size considerations in pattern recognition practice", in *Classification pattern recognition and reduction of dimensionality*, Vol. 2, *Handbook of Statistics* (Elsevier, 1982), pp. 835–855.
- ⁴⁴I. E. Castelli, D. D. Landis, K. S. Thygesen, S. Dahl, I. Chorkendorff, T. F. Jaramillo, and K. W. Jacobsen, "New cubic perovskites for one- and two-photon water splitting using the computational materials repository", *Energy & Environmental Science* **5**, 9034 (2012).
- ⁴⁵I. E. Castelli, J. M. García-Lastra, F. Hüser, K. S. Thygesen, and K. W. Jacobsen, "Stability and bandgaps of layered perovskites for one- and two-photon water splitting", *New Journal of Physics* **15**, 105026 (2013).
- ⁴⁶M. Pandey and K. W. Jacobsen, "Promising quaternary chalcogenides as high-band-gap semiconductors for tandem photoelectrochemical water splitting devices: a computational screening approach", *Physical Review Materials* **2**, 10.1103/physrevmaterials.2.105402 (2018).
- ⁴⁷C. Kim, T. D. Huan, S. Krishnan, and R. Ramprasad, "A hybrid organic-inorganic perovskite dataset", *Scientific Data* **4**, 170057 (2017).
- ⁴⁸G. E. Hinton, "Reducing the dimensionality of data with neural networks", *Science* **313**, 504–507 (2006).
- ⁴⁹L. Ward, R. Liu, A. Krishna, V. I. Hegde, A. Agrawal, A. Choudhary, and C. Wolverton, "Including crystal structure attributes in machine learning models of formation energies via voronoi tessellations", *Physical Review B* **96**, 10.1103/physrevb.96.024104 (2017).
- ⁵⁰L. Himanen, M. O. Jäger, E. V. Morooka, F. F. Canova, Y. S. Ranawat, D. Z. Gao, P. Rinke, and A. S. Foster, "DScribe: library of descriptors for machine learning in materials science", *Computer Physics Communications* **247**, 106949 (2020).
- ⁵¹J. Even, L. Pedesseau, J.-M. Jancu, and C. Katan, "Importance of spin-orbit coupling in hybrid organic/inorganic perovskites for photovoltaic applications", *The Journal of Physical Chemistry Letters* **4**, 2999–3005 (2013).

- ⁵²Y. Hinuma, A. Grüneis, G. Kresse, and F. Oba, “Band alignment of semiconductors from density-functional theory and many-body perturbation theory”, *Physical Review B* **90**, 10.1103/physrevb.90.155405 (2014).
- ⁵³I. E. Castelli, T. Olsen, S. Datta, D. D. Landis, S. Dahl, K. S. Thygesen, and K. W. Jacobsen, “Computational screening of perovskite metal oxides for optimal solar light capture”, *Energy Environ. Sci.* **5**, 5814–5819 (2012).
- ⁵⁴M. F. Langer, A. Goeßmann, and M. Rupp, “Representations of molecules and materials for interpolation of quantum-mechanical simulations via machine learning”, (2020).
- ⁵⁵C. J. Willmott and K. Matsuura, “Advantages of the mean absolute error (mae) over the root mean square error (rmse) in assessing average model performance”, *Climate Research* **30**, 79–82 (2005).
- ⁵⁶J. Schrier, “Can one hear the shape of a molecule (from its coulomb matrix eigenvalues)?”, *Journal of Chemical Information and Modeling* **60**, 3804–3811 (2020).
- ⁵⁷M. C. Hemmer, “Radial distribution functions in computational chemistry - theory and applications”, PhD thesis (Friedrich-Alexander-Universität Erlangen-Nürnberg, Apr. 26, 2007).
- ⁵⁸L. van der Maaten and G. Hinton, “Visualizing high-dimensional data using t-sne”, English, *Journal of Machine Learning Research* **9**, Pagination: 27, 2579–2605 (2008).
- ⁵⁹M. Wattenberg, F. Viégas, and I. Johnson, “How to use t-SNE effectively”, *Distill* **1**, 10.23915/distill.00002 (2016).
- ⁶⁰S. Tao, I. Schmidt, G. Brocks, J. Jiang, I. Tranca, K. Meerholz, and S. Olthof, “Absolute energy level positions in tin- and lead-based halide perovskites”, *Nature Communications* **10**, 10.1038/s41467-019-10468-7 (2019).
- ⁶¹P. Borlido, T. Aull, A. W. Huran, F. Tran, M. A. L. Marques, and S. Botti, “Large-scale benchmark of exchange–correlation functionals for the determination of electronic band gaps of solids”, *Journal of Chemical Theory and Computation* **15**, PMID: 31306006, 5069–5079 (2019).
- ⁶²M. M.-C. Vidovic, N. Görnitz, K.-R. Müller, G. Rättsch, and M. Kloft, “Opening the black box: revealing interpretable sequence motifs in kernel-based learning algorithms”, in *Machine learning and knowledge discovery in databases* (Springer International Publishing, 2015), pp. 137–153.
- ⁶³J. Gilmer, S. S. Schoenholz, P. F. Riley, O. Vinyals, and G. E. Dahl, “Neural message passing for quantum chemistry”, in *Proceedings of the 34th international conference on machine learning - volume 70, ICML’17* (2017), pp. 1263–1272.
- ⁶⁴O. Rahaman and A. Gagliardi, “Deep learning total energies and orbital energies of large organic molecules using hybridization of molecular fingerprints”, 10.26434/chemrxiv.12581381.v1 (2020).
- ⁶⁵C. W. Park and C. Wolverton, “Developing an improved crystal graph convolutional neural network framework for accelerated materials discovery”, (2019).

⁶⁶M. Banko and E. Brill, “Scaling to very very large corpora for natural language disambiguation”, in Proceedings of the 39th annual meeting on association for computational linguistics - ACL '01 (2001).